# ENHANCED UNIPOLAR OFDM BASED RELAY-ASSISTED VISIBLE LIGHT COMMUNICATIONS

A Thesis

by

Djengomemgoto Gerard

Submitted to the
Graduate School of Sciences and Engineering
In Partial Fulfillment of the Requirements for
the Degree of

Master of Science

in the
Department of Electrical and Electronics Engineering

Özyeğin University
August 2016

# ENHANCED UNIPOLAR OFDM BASED RELAY-ASSISTED VISIBLE LIGHT COMMUNICATIONS

Approved by:

---

Professor Dr. Murat Uysal, Advisor
Department of Electrical and Electronics Engineering
*Özyeğin University*

---

Assistant Professor Dr. Cenk Demiroğlu
Department of Electrical and Electronics Engineering
*Özyeğin University*

---

Assistant Professor Dr. Tunçer Baykaş
Department of Computer Engineering
*Medipol University*

Date Approved: 5 August 2016

*To my dearest parents, siblings and friends.*

*To my beloved Teihissande Tingolfa.*

# ABSTRACT

Due to spectrum scarcity of the conventional radio frequency (RF) and the higher demand for wireless services, visible light communication (VLC) has emerged as a complementary solution to RF technology for ubiquitous wireless connectivity. In the first part of this thesis, we consider a relay-assisted VLC system in an indoor environment where an intermediate light source cooperates with the main light source through an orthogonal amplify-and-forward (OAF) relaying protocol in order to transmit high-speed data to the destination terminal. The optical channel considered in this scenario is based on the IEEE802.15.7r VLC reference channel model for an office space. The information source (ceiling light) is connected to the backbone network, desk light acts as a relaying terminal and the receiving terminal is a photodetector attached to a computer. All the three network terminals are equipped with signal-processing units. The proposed relay-assisted VLC system employs the enhanced unipolar optical orthogonal frequency division multiplexing (eU-OFDM) modulation approach. Our performance results show that the relay-assisted system achieves a significant gain over the direct transmission. In the second part of this thesis, a serial multi-hop VLC network is considered. We evaluate the BER performance analysis of multi-hop VLC links through Monte Carlo simulation and validate the simulation results with their respective theoretical counterparts.

# ÖZETÇE

Radyo frekansı (RF) spektrumu kablosuz servislere artan ihtiyacı karşılayamaz duruma gelmiş olup tamamlayıcı bir çözüm olarak görünür ışık haberleşmesi (Visible Light Communication − VLC), ortaya çıkmıştır. Tezin ilk kısmında, bir içmekanda çalışan röle-destekli VLC sistemi ele alınmıştır. Sözkonusu sistemde ortogonal yükselt-ve-gönder (amplify-and-forward − OAF) röleleme protokolu kullanılmakta ve bir ara ışık kaynağı ana ışık kaynağına yüksek hızda veri iletimi için yardımcı olmaktadır. Optik kanal modeli olarak ofis senaryoları için önerilmiş IEEE802.15.7r VLC referans kanal modeli kullanılmıştır. Bilgi kaynağı (tavan ışığı) omurga ağına bağlı olup, masa lambası ise röle terminali olarak görev almaktadır ve alıcı terminal bir bilgisayara yerleştirilmiş olan bir fotodetektördür. Üç ağ terminaline de birer sinyal işleme birimi konulmuştur. Önerilen röle-destekli VLC sistemi, gelişmiş tek kutuplu optik ortogonal frekans bölmeli çoğullama (enhanced unipolar optical orthogonal frequency division multiplexing − eU-OFDM) tekniği kullanmaktadır. Başarım sonuçlarımız önerilen röle destekli sistemin, doğrudan iletime göre ciddi ölçüde kazançlar sağladığını göstermektedir. Tezin ikinci kısımında, çok-atlamalı bir VLC ağı gözönüne alınmıştır. Çok atlamalı VLC ağı için bit hata oranı başarımı analizi yapılmış ve Monte Carlo simülasyon sonuçları ile doğrulanmıştır.

# ACKNOWLEDGEMENTS

I would like to express my sincere gratitude and appreciation to my thesis advisor, Professor Dr. Murat Uysal, for his continuous guidance, patience, care and endless support throughout my thesis and my graduate studies at Özyeğin University. His thoughtful comments, insightful feedback and meticulous suggestions have been paramount in producing a high-quality research project. I am also thankful for being a part of his CT&T research group.

I would like also to thank Ömer Narmanlıoğlu for his valuable help and time, and for all the constructive discussions we have had throughout this thesis. It was really a great experience and an immense pleasure to have worked with you.

To all my colleagues from CT&T research lab (Mohammed, Farshad, Hatef, Mohammad, Alireza, Maryam and Hamed), thank you all for your friendship, love and care. My thanks go also to Anil and Burak for their help in translating the abstract of my thesis.

I am especially indebted to Erkan Kemal, Dr. Buse Yilmaz, Mirza Awais Ahmad and all my amazing and great friends from OzU, thank you all for your friendship and for giving me a memorable graduate school experience. I would like to express my thanks to Issa Abderamane and Narcisse Mbairamadji. Your friendship, encouragement and support have helped me to keep going during tough times.

I would like also to express my deepest sense of gratitude to my dearest parents, to my dearest brothers and sisters, to my beloved Teihissande Tingolfa for their endless love, care, encouragement and support throughout my stay and studies in Turkey. I could not have done it without you. Finally, my thanks go also to the Almighty for giving the strength during tough times and throughout my graduate studies.

# TABLE OF CONTENTS

# LIST OF TABLES

# LIST OF FIGURES

# CHAPTER I

# INTRODUCTION

This chapter presents a brief review of optical wireless communications and presents the concept of visible light communication by reviewing the the fundamental theories of optical sources, indoor VLC links and optical receivers. The state-of-the-art on multi-carrier modulation techniques for intensity modulation/direct detection systems and the use of cooperative relaying techniques in VLC are further discussed. In reference to these, the thesis motivation and contribution are also discussed in this chapter.

## *1.1 Optical Wireless Communications*

Wireless communication systems are predominantly based on radio frequency (RF) technology. In RF-based wireless communication, the information is carried through the wireless medium in the form of radio waves. These radio waves are spanned by the RF spectrum which goes from 30 kilohertz (kHz) to 300 gigahertz (GHz). However, the spectrum allocation within this RF band is regulated at both national and international level and a license is required in order to use a sub-band of this scarce resource [2]. The licensing and regulation of this resource help to guarantee efficient use and equitable access to wireless services.

With the exponential growth of mobile and computing devices together with the demand for higher data rate and better wireless service have lead to congestion of RF spectrum [2]. In order to alleviate the burden on RF spectrum, alternative wireless communication technologies have been explored. Particularly, the optical wireless communication (OWC) has recently been the center of attraction in research and development from numerous institutions, organizations and universities across the globe.

This wireless technology relies on the upper band of the electromagnetic spectrum, which spans from infrared (IR) band through visible light (VL) band to ultraviolet (UV) sub-bands. Thus, by definition, OWC refers to transmission in unguided propagation media through the use of optical carriers [3].

The concept of OWC has been around long before the birth of RF-based wireless communication [4], [5]. For example, people used fire and smoke signaling techniques or fire beacons in order to communicate over long distance. In 1791, Claude Chappe′s optical telegraphic system was built and tested with successful transmission of numbers which correspond to words in a French dictionary [4]. Chappe′s invention was followed by the works of Alexander Graham Bell on "photophone" which earned him a U.S patent in 1880 [6], [7]. In the proposed system, Bell made use of reflective mirror surface and beam of sunlight to allow successful transmission of voice signal over the wireless medium.

Since the invention of lasers in 1960, various experimental works on OWC systems have been conducted [8], [3]. However, the experimental demonstrations during the 1960s were problematic because of unreliable optical wireless devices and systems. Consequently, during the 1970s, many have opted for fiber optic technology for long-range OWC [3]. As reported in [9], the first efficient laser diode was introduced in 1980 but the OWC systems were only used by the military from the 1980s through the 1990s [9], [3]. In recent years, with the proliferation of companies offering state-of-the-art optical systems, OWC has emerged as a promising wireless technology [3].

In contrast to RF-based wireless communication, OWC presents several advantages due to its huge amount of bandwidth and inherent attributes [6], [10]. Optical wireless communication is low cost with unregulated spectrum, license free and broad optical spectrum. In addition, the optical radiation cannot propagate or pass through opaque objects or walls like radio frequencies. This is an interesting feature for OWC systems in term of network and information security as it helps to easily scrutinize,

identify and avoid eavesdropping. In an outdoor optical network scenario (i.e.,free space optical communication) for example, the optical transmitter and receiver can be geometrically and geographically positioned to form a line-of-sight (LOS) link so that any intervening obstruction or eavesdroppers can be easily detected. For the case of an indoor environment, the optical signal can be confined within a specific room or office space thus providing secure data transmission and reception while also eliminating the plausible interfering signals from neighboring indoor spaces.

Also, the optical hardware is more energy-efficient than their RF counterparts and they do not cause interference with RF sensitive devices used in areas such as hospitals or aircraft cabins. Moreover, OWC does not suffer from multipath fading since the size of the detector, which is larger than the wavelength of the light, enables the optical system to exploit the spatial diversity [10].

Although the advantages of optical wireless communication make this communication technology undoubtedly very promising, OWC exhibits also some disadvantages. Outdoor OWC systems are prone to weather conditions, atmospheric turbulences and sunlight or ambient light. Additionally, for eye safety requirements, the transmitted optical power is also limited. Consequently, the requirement to comply with eye safety regulations leads to greater complexity in optical system design and they limit also the coverage of OWC systems. Due to these safety reasons, lasers are only intended for outdoor applications while LEDs are used for indoor optical wireless communication.

Optical wireless communication can be categorized as free space optical (FSO) communication, visible light communication (VLC) and ultraviolet communication (UVC). FSO is intended for short to long-range applications, VLC is used for indoor or, in some cases, short range outdoor applications while UVC is for short-range outdoor application involving non-line-of-sight (NLOS) communications [11].

## 1.2 Free Space Optical Communications

Revolutionized by the invention of lasers in the 1960s, FSO communication has evolved into maturity, at some extent, compared to UVC and VLC. FSO systems operate in the infrared (IR) region between 750 nm to 1600 nm in wavelength. This branch of optical wireless communication relies on the laser diodes (LDs), which present a highly directional pattern and exhibit higher power compared to light emitting diodes (LEDs), to transmit high speed data to receiving end or photodetector (PD). Although FSO communication systems have already been deployed to support data transmission between two fixed points [3], their link reliability is still a problem for moving or flying objects and targets such as unmanned aerial vehicles Therefore, tracking mechanisms are required in optical systems in order to efficiently use the FSO link [12].

The ease in the installation of FSO systems makes this technology a promising candidate for application in terrestrial based public safety network [2]. The latter becomes crucial during natural disasters such as hurricanes or tsunamis. During these catastrophic events, when the network infrastructures in some affected locations are down, the public safety agencies and emergency workers may experience serious problems in establishing wireless connection since the remaining functional parts of the network may be unable to cope with the traffic demand. In this case, FSO systems can be quickly deployed for the reestablishment of the network so that crisis can be better managed during these disastrous events. Similarly, FSO can also provide network access to remote areas. Other current and potential applications of this optical wireless technology are described in details in [2], [3] and [13].

## 1.3 Ultraviolet Communications

Ultraviolet communication is one the emerging branches of OWC technology as a result of new developments in the area of solid state optical components. The

ultraviolet band spans from 4 nm to 400 nm in wavelength. However, only the UV-C band which spans from 200 nm to 280 nm is used for UVC [2], [11], [14]. Ultraviolet communication is possible for both LOS and NLOS communications within this mid-UV band because of its exceptional scattering diversity, channel and propagation characteristics as reported in [14]. The scattering diversity makes UVC links less affected by the background noise compared to FSO links in non-line-of-sight channels. However, the attenuation experienced by UVC over NLOS links is more dominant compared to LOS channels.

In addition, for the purpose of eye and skin safety requirements, the power emitted by UVC sources is strictly limited. Consequently, ultraviolet communication is good for short range NLOS applications or sensing networks.

## *1.4 Visible Light Communications*

The recent advances and breakthroughs in solid-state lighting have led to the development and deployment of energy efficient LEDs with longer luminaire lifespan [15] compared to the conventional incandescent light bulbs. LEDs have not only revolutionized the field of illumination technology but they have also sparked tremendous research effort in the area of VLC [16], [17]. VLC is a low-cost, secure and energy efficient technology with unregulated spectrum that uses light from the increasingly popular light emitting diodes for high throughput data transmission and it causes no interference with the existing RF-based systems [16].

Due to spectrum scarcity of the conventional radio frequency together with the higher demand for wireless services, visible light communication, with its distinct features and great prospects, has been proven to be one of the vital and ultimate complementary solutions to the existing RF technology for ubiquitous wireless connectivity [17], [18]. In addition, the visible light spectrum lies between 380 nanometers (nm) to 750nm in wavelength, consequently VLC systems are intended for short range

applications [19], [20].

According to recent studies on wireless usage [21], 50% of voice calls and a greater portion ($> 70\%$) of all data traffics originates indoors. VLC for indoor environment can help in alleviating the burden on RF spectrum while providing better connectivity for indoor users without causing interference to the outdoor users [16].

In a typical VLC system, LEDs are used as transmitters while PDs handle the signal reception. With the state-of-the-art illumination, light or image sensor technologies and based on the currently available off-the-shelf LEDs and photodetectors, VLC systems are built using intensity modulation and direct detection (IM/DD) scheme.

### 1.4.1 VLC Source: Light Emitting Diode

By definition, an LED is a semiconductor $p$-$n$ junction device that gives off spontaneous optical radiation when subjected to electronic excitation [6]. In VLC, white LEDs are used as optical sources because of their ability to emit light within 400 nm to 700 nm in wavelength [22]. White LEDs are fabricated through two different approaches: phosphor based approach and tri-chromatic or RGB based approach. In phosphor based approach, a white LED is generated by coating a blue LED with a yellow phosphor layer. Although this approach is cheaper and less complex, it leads to a slight shift in wavelength. The second approach involves the combination of red ($\sim$ 625 nm), green (525 nm) and blue (470 nm) LEDs (also referred to as RGB approach) in order to generate white LED. The use of three different LEDs to produce white LEDs increases the production cost compared to the first approach. However, the tri-chromatic approach offers the white LEDs with attractive characteristics and features in term of wavelength division multiplexing. It also enables color control and high speed data transmission [6], [22].

LEDs are low power and energy efficient compared to LDs and they fulfill eye

and skin safety requirements. Thus, LEDs can be safely used for indoor optical wireless networks without impeding their primary usage for illuminations. At the transmitting end, LEDs also perform intensity modulation by handling the electro-optical conversion of the signal to be transmitted. As a result, the signal used to drive the LEDs must be real and positive value. In addition, they present also a limited modulation bandwidth in the order of megahertz (MHz) [22]. An extended literature on the technology of LEDs is presented in [6], [22] and [23].

### 1.4.2 VLC Receiver: Photodetector

Photodetectors are used as optical receivers for VLC systems to detect the optical intensity and perform the opto-electrical (O/E) conversion of the received signal [7]. The performance of a PD depends on its attenuation coefficient or quantum efficiency $\eta$. The quantum efficiency of a photodetector is defined as [6], [7], [22], [23]

$$\eta = \xi \left(1 - R_e\right) \left(1 - e^{-\alpha d}\right) \tag{1}$$

where $R_e$ refers to reflection coefficient and it indicates the percentage of reflected incident power at the surface of PD, $\xi$ is the ratio of electron-hole pairs that contribute to useful photocurrent,$\alpha$ defines the absorption coefficient ($\mathrm{cm}^{-1}$) and $d$ is the photodetector's depth.

After O/E conversion, the instantaneous photocurrent is [6], [7], [22], [23]

$$i\left(t\right) = \eta \frac{q\lambda P\left(t\right)}{hc} = RP\left(t\right) \tag{2}$$

where $P\left(t\right)$ is the received instantaneous average power at PD, $q$ denotes the electron charge, $h$ is Plank's constant, $c$ is the speed of light, $\lambda$ refers to wavelength ($\mu$m) and $R$ is the responsivity $(A/W)$ of the photodetector.

The responsivity of the photodetector is the ratio of instantaneous photocurrent $i\left(t\right)$ and the instantaneous incident power $P\left(t\right)$. In other word, $R$ refers to the opto-electrical conversion efficiency of the photodetector and it is given by

$$R = \frac{i\,(t)}{P\,(t)} = \eta\frac{q\lambda}{hc} = \frac{\lambda}{1.24}\eta \tag{3}$$

### 1.4.3 VLC Channel Model and Configurations

Based on the propagation paths of the transmitted light beam through the indoor optical channel, the VLC link can be categorized as LOS and NLOS channel configurations [6], [22], [7]. In LOS link configuration, the path from LED to PD's field-of-view is unobstructed, the emitted light beam can travels through the channel and reach directly the optical receiver. This channel configuration can be further classified as either directed LOS or non-directed LOS [6]. The latter is for indoor applications where the LED emits a wide beam and the FOV of the photodetector is wide for a broader coverage.

However, the directed LOS channel configuration is for outdoor or indoor applications requiring point-to-point transmission. In this channel configuration, the source emits a narrow beam of light and the FOV of the PD is also narrow. In NLOS channel configuration, the optical signal may bounce from different surface materials within the indoor environment, such as ceiling or wall, before reaching the detector [6]. Similar to LOS, the NLOS link can be either directed or non-directed (diffuse) as described in [10]. There are also some hybrid VLC link configurations in which the optical receiver tracks the directed light beam. The fundamental VLC channel configurations for indoor environment is portrayed in Figure 1.

In indoor optical wireless communication system, the photocurrent $i\,(t)$ is emitted from the LED and it travels through the optical channel to the photodetector. The electro-optical conversion can be modeled as $i\,(t) = g_o x\,(t)$, where $g_o$ is the optical gain. Throughout this thesis, this optical gain is set to unity, for convenience. Let the detected signal at the photodetector be denoted by $y\,(t)$ and the channel impulse response (CIR) of the IM/DD-based system be $h\,(t)$. The channel model for indoor

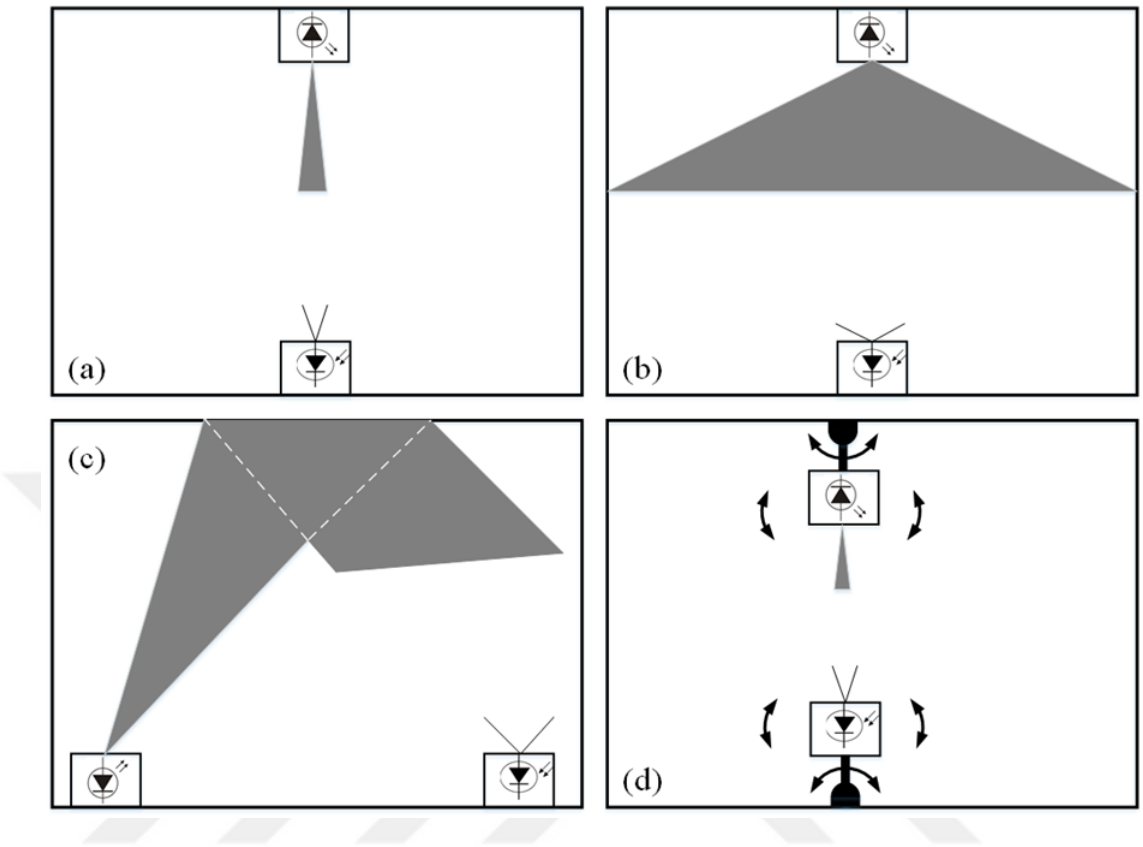


**Figure 1:** VLC link configurations: (a) directed LOS, (b) nondirected LOS, (c) diffuse, (d) tracked.

VLC is depicted in Figure 2.

The received signal is then given by

$$y(t) = Rh(t) \otimes x(t) + n(t) \tag{4}$$

where $R$ is the photodetector responsivity $(A/W)$, $\otimes$ denotes the convolution operation. and $n(t)$ is modelled as an additive white Gaussian noise (AWGN).

Due to IM/DD constraints, the resulting optical signal $x(t)$ must be positive and real-value signal, its instantaneous power should not exceed the maximum allowable power $P_{\max}$ for eye safety compliance. Therefore, we have [7]

$$x(t) \geq 0, \ \forall \ t \ \in \ \mathbb{R} \tag{5}$$

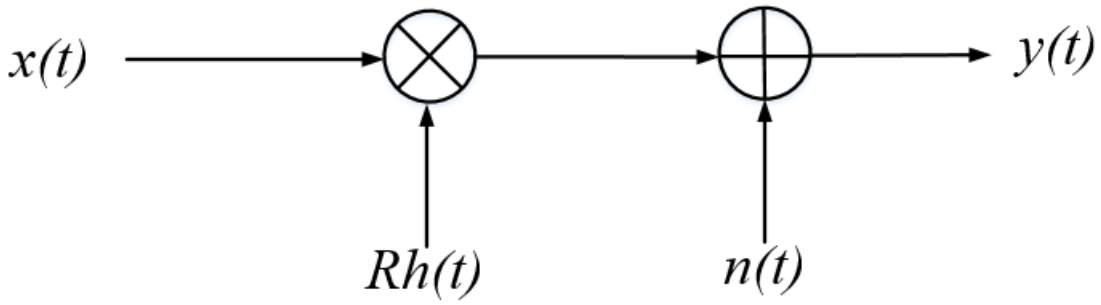


**Figure 2:** VLC channel model

$$\lim_{T\to\infty} \frac{1}{2T} \int_{-T}^{T} x\left(t\right) dt \leq P_{\max} \tag{6}$$

## *1.5 Multi-Carrier Modulation in VLC*

In a typical VLC system, intensity modulation and direct detection (IM/DD) schemes are used where information is encoded with the light intensity while photodetectors handle the signal reception. Under this scheme, the information waveform needs to be real and positive valued. These constraints limit the usage of conventional complex or bipolar modulation schemes used in RF-based systems. Initial works in VLC considered simple pulse modulation techniques such as on-off keying (OOK) pulse position modulation (PPM) [24].

Recent studies [25] - [26] have adopted orthogonal frequency division multiplexing (OFDM) for optical systems. Conventional OFDM structure, however, cannot be directly applied to VLC or IM/DD systems.

Consequently, different optical OFDM such as asymmetrically clipped optical OFDM (ACO-OFDM) [25], Unipolar OFDM (U-OFDM) [27] or Flip-OFDM [28], DC biased optical OFDM (DCO-OFDM) [29], enhanced unipolar OFDM (eU-OFDM) [26] have been proposed. It is important to note also that, for the purpose of overcoming

the constraints of IM/DD systems, all these optical OFDM techniques generate real-value signals by imposing the Hermitian symmetry property on the complex symbol vector at the input of $N$-point inverse discrete Fourier transform ($N$-IDFT).

In ACO-OFDM [25], the complex data symbols are carried only on the odd indexed subcarriers. Based on this structure, for a signal vector to the input of $N$-point IDFT, only $N/4$ data symbols are used for encoding. The negative parts of the output of IDFT are then clipped without affecting the original data; the clipped signal is then used for transmission through the optical system. As a result, the data rate of ACO-OFDM is given by [30]

$$R_{ACO} = \left[\frac{N/4}{N + N_{CP}}\right] B\log_2(M) \ \ (bps) \tag{7}$$

where $B$ is the bandwidth (Hz), $N_{CP}$ is the length of cyclic prefix and $M$ is the constellation size for QAM or PSK modulation scheme.

Similarly, the frame construction for U-OFDM [27] or Flip-OFDM [28] is done by encoding $N/2-1$ data symbols. After $N$-point IDFT process, the resulting data vector undergoes two processes in order to produce two positive data sub-frames. The first sub-frame is obtained by setting all negative components of IDFT output vector to zeros. The second sub-frame is formed by flipping (inverting the polarity) of IDFT output prior to clipping the signal. The two sub-frames are then consecutively transmitted through the IM/DD system. Since the encoded $N/2-1$ data in the original signal is transmitted in two different sub-frames, U-OFDM and Flip-OFDM present almost similar spectral efficiency (SE) and the same bit error rate as ACO-OFDM. Their relative achievable data rate is given by

$$R_U = \left[\frac{N/4 - 1/2}{N + N_{CP}}\right] B\log_2(M) \ \ (\text{bps}) \tag{8}$$

As for the case of DCO-OFDM [29], the frame structure is formed by rearranging the $N/2-1$ data symbols. In this optical OFDM scheme, a DC-bias is added to the

output of $N$-point IDFT in order to get unipolar signal at the input of LED. The additional DC-bias makes this scheme energy-inefficient compared to ACO-OFDM and Flip-OFDM (or U-OFDM). DCO-OFDM, however, achieves higher SE than ACO-OFDM and Flip-OFDM schemes. The achievable data rate for DCO-OFDM is defined as [30]

$$R_{DCO} = \left[\frac{N/2-1}{N+N_{CP}}\right] B\log_2(M) \ \ (bps) \tag{9}$$

In order to approach the spectral efficiency of DCO-OFDM without the need of using additional power, enhanced unipolar OFDM (eU-OFDM) has been proposed recently [26]. This new multi-carrier technique makes use of different depths (layers) where independent streams of data can be duplicated with respect to the corresponding depth number, summed and transmitted as a single frame. This scheme presents a 95.88% spectral of efficiency of DCO-OFDM for a maximum depth of 5.

## *1.6 Relay-Assisted VLC*

Relaying techniques have been proven to improve the performance of both RF-based [31] and VLC systems [32]-[33] compared to the performance of a direct (point-to-point) link. In [32], the author combined DCO-OFDM with relaying schemes and demonstrated a good performance gain of the relay-assisted system under illumination constrain. Similarly, reference [34] employed power allocation strategy to show the BER performance of the system and a significant gain was achieved with optimum power allocation. ACO-OFDM and DCO-OFDM have been used to test the performance of a relay-assisted system presented in [33] for both AWGN channel and a realistic indoor VLC channel.

Based on the literature, the relay-assisted VLC systems for indoor environment is still at its infancy. Therefore, more research works need to be done in order to enable this emerging optical communication technology to reach its potentials. The key contributions in this thesis are twofold.

In the first part, we adopt the newly proposed eU-OFDM and the orthogonal amplify and forward (AF) relaying protocol [35] in order to evaluate the performance of the indoor VLC system based on the IEEE802.15.7r channel model presented in [1] for different modulation orders. The relay-assisted VLC system performance can then be used to conduct a comparative study with the performance of a point-to-point system which is used as benchmark.

In the second part of this thesis, we consider a serial multi-hop relay-assisted VLC link and analyze its performance based on eU-OFDM scheme. In the considered VLC network scenario, multiple users are located sequentially so that the data can be forwarded from one user to another through multi-hop AF relaying protocol. Based on this network topology, we provide the SNR and BER expressions for each user node. Monte Carlo simulations results are then validated by their theoretical counterparts.

## *1.7 Organization of the Thesis*

Chapter II presents the modeling of the eU-OFDM based relay-assisted VLC system model and its performance analysis. The eU-OFDM based multi-hop relay-assisted VLC networks are described and analyzed in Chapter III. Chapter IV concludes the thesis.

**Notation:** $(.)^*$ and $[.]^{\mathrm{T}}$ denote complex conjugate and transpose, respectively. $\mathbf{E}\{.\}$ denotes the statistical averaging and $Q(.)$ is the tail probability of standard normal distribution.

# CHAPTER II

# eU-OFDM BASED RELAY-ASSISTED VLC SYSTEM

This chapter briefly describes the VLC channel model based on a realistic indoor environment. The channel impulse responses for both point-to-point and relay-assisted transmissions are also presented. Using the system models based on eU-OFDM, their respective theoretical signal-to-noise ratio (SNR) and bit error rate (BER) are derived and analyzed. The performance measurement and evaluation of each VLC system are highlighted.

## *2.1 Indoor VLC Channel Model Based on IEEE Standard*

We use the reference channel model (see Figure 3) adopted by IEEE 802.15.7r Task Group Short Range Optical Wireless Communication [1]. In order to obtain the optical channel impulse responses (CIRs), we consider an indoor office environment with room dimensions of 5m×5m×3m. For the relaying system configuration, the information source (ceiling light) is assumed to be connected to the backbone network, the desk light acts as a relaying terminal and the destination is the photodetector connected to laptop. All the system terminals are equipped with digital signal processing (DSP) units. The coordinates of the relaying system are accordingly set as follow. The coordinates of the optical source (LED) and the receiver (PD) are set to (0, 0, 3) and (−1.19, 1.35, 0.88), respectively. The locations of relay LED and the relay PD are correspondingly set to (−1.26, 1.28, 1.5) and (−1.19, 1.35, 1.33). The center of the ground is set to (0, 0, 0). The indoor room environment for an office space is depicted in Figure 3.

The half viewing angles of LEDs are set to $40^o$ and a $1cm^2$ photodetector with field-of-view (FOV) of $85^o$ is considered. The channel impulse responses (CIRs) from

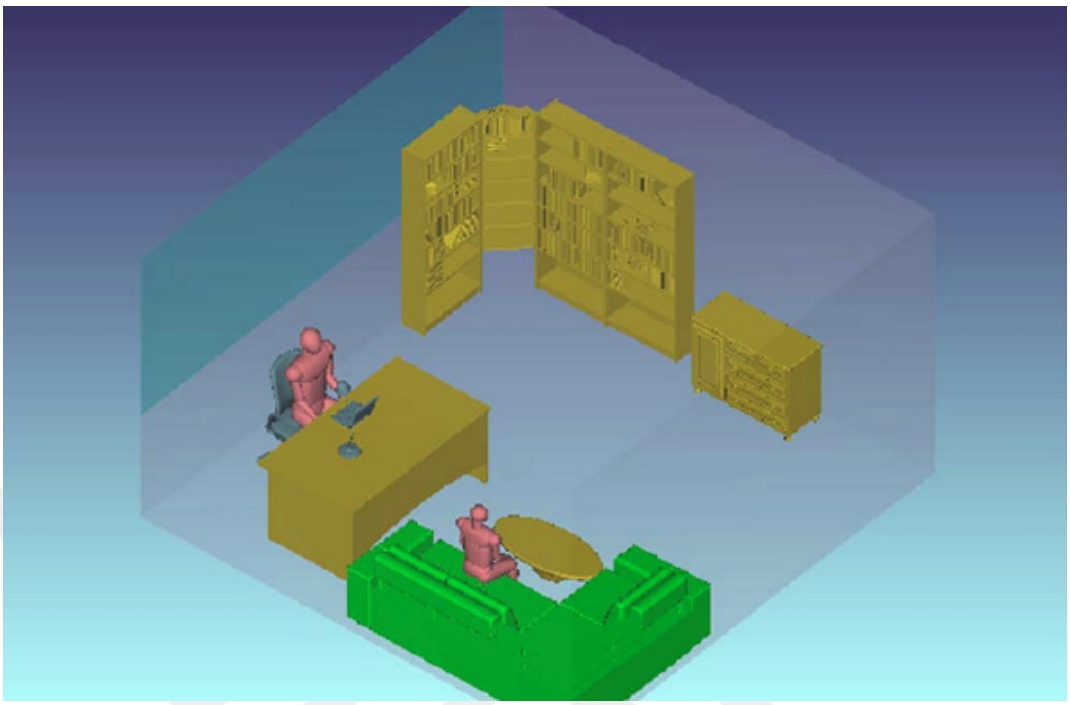

**Figure 3:** Simulated office environment [1].

source to destination ($S \rightarrow D$ path), from source to relay ($S \rightarrow R$ path) and from relay to destination ($R \rightarrow D$ path) are denoted by $h_{SD}(t)$, $h_{SR}(t)$ and $h_{RD}(t)$, respectively. Figure 4 - Figure 6 depict the CIRs of the system. A square root raised cosine pulse shape with unity excess bandwidth parameter is assumed. Under this assumption, for a given CIR $c_{AB}(t)$ and with transmit and receive pulse shaping filters $g_A(t)$ and $g_B(t)$, the band-limited channel response from terminal $A$ to terminal $B$ can be written as

$$h_{AB}(t) = g_A(t)\, c_{AB}(t)\, g_B(t) \tag{10}$$

## *2.2 System Model*

In this section, the system model for direct transmission is first described for benchmark purposes. The relay-assisted VLC system is then modeled by using the orthogonal AF relaying technique.

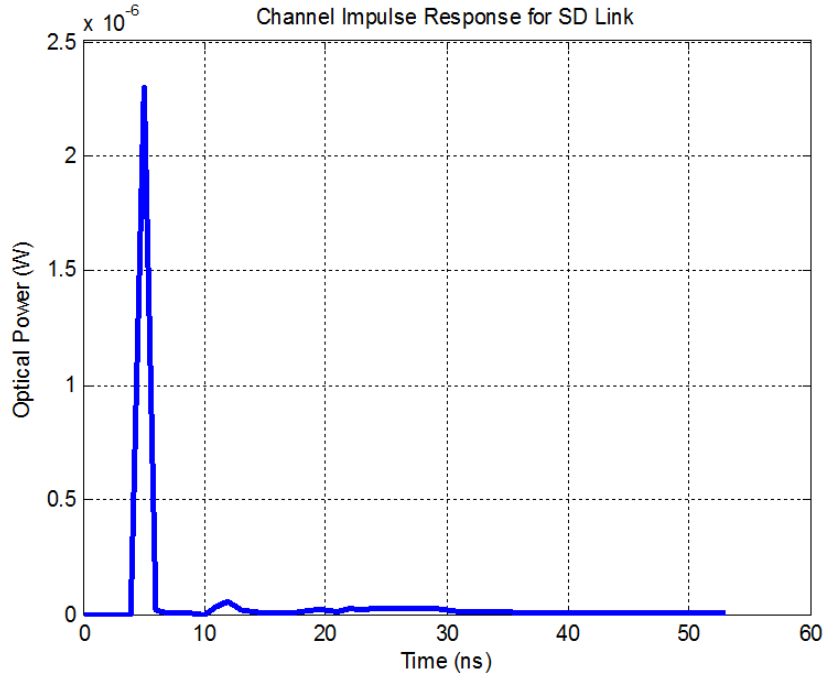


**Figure 4:** CIR for source to destination terminal.

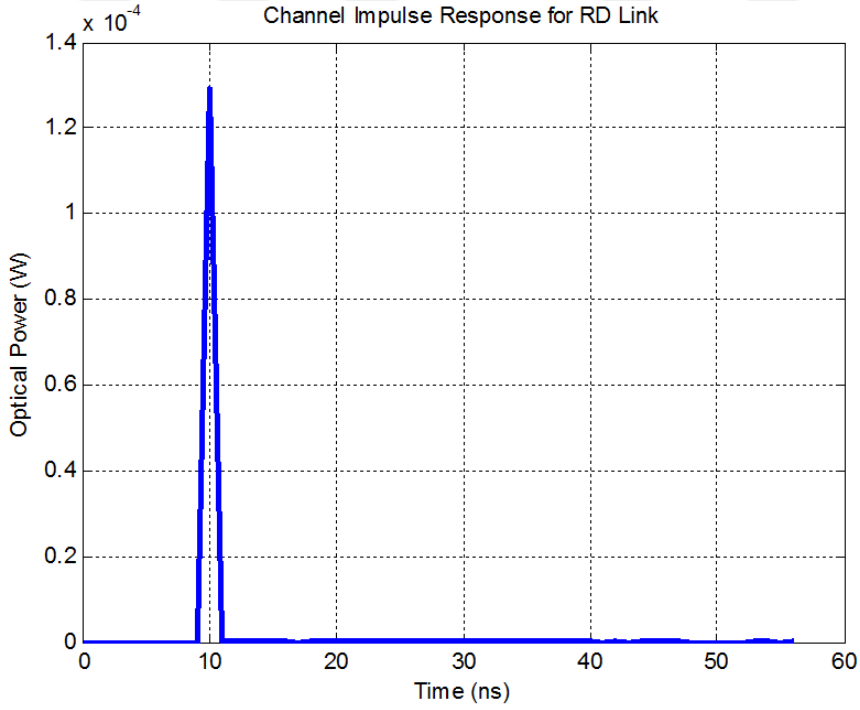


**Figure 5:** CIR for source to relay terminal.

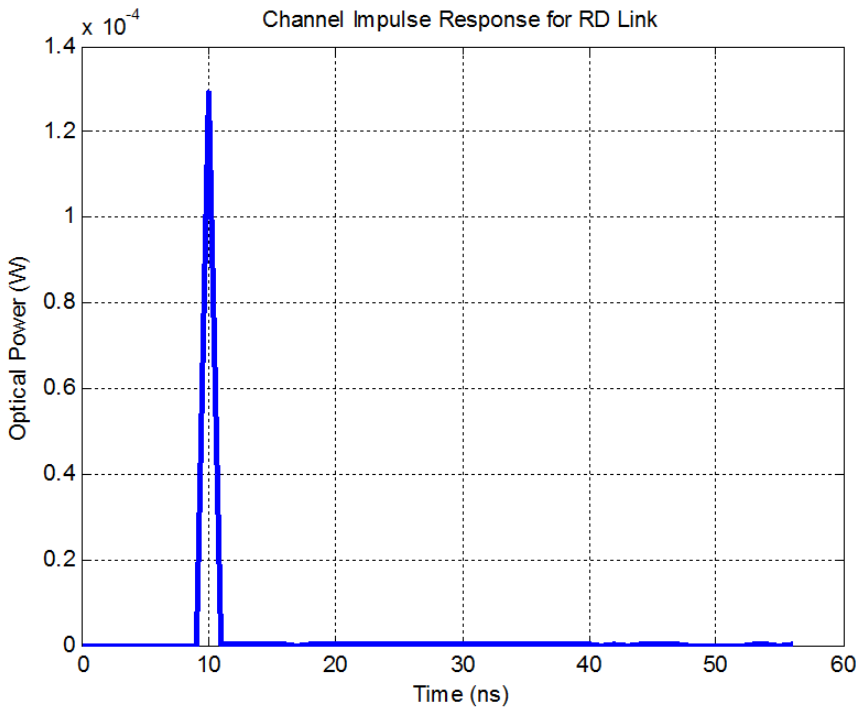


**Figure 6:** CIR for relay node to destination terminal.

### 2.2.1 Direct Transmission

We consider eU-OFDM for the physical layer aspect of proposed system structure. Let $\left(s_1\ s_2\ ...\ s_{N/2-1}\right)$ with the average energy of $E$, be the $M-$ary quadrature amplitude modulation (QAM) or phase shift keying (PSK) complex data symbols to be transmitted through the VLC system. The size of the modulated data symbols is similar to that of U-OFDM $(N/2-1)$. Thus, prior to IDFT of size $N$, the stream of modulated complex data symbols is subjected to Hermitian symmetry in order to obtain real-value signals. The rearranged data structure is written as

$$\mathbf{X} = \left[0\ s_1\ s_2\ s_3\ ...\ s_{N/2-1}\ 0\ s^*_{N/2-1}\ ...\ s^*_2\ s^*_1\right]^{\mathrm{T}}. \tag{11}$$

The real-valued signal resulting from the $N-$point IDFT sequence is defined as

$$x[n] = \frac{1}{\sqrt{N}} \sum_{k=0}^{N-1} X[k] e^{j\frac{2\pi nk}{N}}. \tag{12}$$

The U-OFDM data sequences are then used to build the eU-OFDM frame prior

to prepending the data with cyclic prefix (CP) whose length is denoted by $N_{CP}$. For a given maximum depth of $U$ (with $d = 1, 2, ..., U$), the eU-OFDM frame is formed by summing the data arrays from $U$ layers. The first layer of data (first depth) follows the structure of U-OFDM. For the subsequent depths ($d > 1$), each U-OFDM data sequence at depth $d$ is duplicated $2^{d-1}$ times and scaled by a factor of $1/\sqrt{2^{d-1}}$ in order to keep the energy per symbol constant. The data sequences from all depths undergo a data array summation and the resulting data vector is the eU-OFDM symbol. This data symbol goes through parallel to serial conversion and digital-to-analog conversion prior to transmission via the optical link. As an illustration, the frame structure of eU-OFDM for a maximum depth of three is shown in Figure 7. By setting the spectral efficiency (SE) of the first to 1 bit/s/Hz, then the SEs of $2^{nd}$ and $3^{rd}$ depths become 0.5 and 0.25 bit/s/Hz, respectively.

| | | | | | | | | | | | | | | | | | | | | |
|---|---|---|---|---|---|---|---|---|---|---|---|---|---|---|---|---|---|---|---|---|
| D1: | Neg. $x_{14}$ | CP | Pos. $x_{14}$ | CP | Neg. $x_{13}$ | CP | Pos. $x_{13}$ | CP | Neg. $x_{12}$ | CP | Pos. $x_{12}$ | CP | Neg. $x_{11}$ | CP | Pos. $x_{11}$ | CP |
| D2: | Neg. $x_{22}$ | CP | Neg. $x_{22}$ | CP | Pos. $x_{22}$ | CP | Pos. $x_{22}$ | CP | Neg. $x_{21}$ | CP | Neg. $x_{21}$ | CP | Pos. $x_{21}$ | CP | Pos. $x_{21}$ | CP |
| D3: | Neg. $x_{31}$ | CP | Neg. $x_{31}$ | CP | Pos. $x_{31}$ | CP | Pos. $x_{31}$ | CP | Neg. $x_{31}$ | CP | Neg. $x_{31}$ | CP | Pos. $x_{31}$ | CP | Pos. $x_{31}$ | CP |

**Figure 7:** eU-OFDM frame structure.

For an eU-OFDM of a maximum depth of $U$, let $x(t)$ denote the resulting time domain signal after summation of all depths. $E_T(U)$ denotes its energy and is given by (13) where $\Theta$ is the probability density function of standard normal distribution and $x_d(t)$ is the transmitted signal in the $d^{th}$ depth [26].

$$E_T(U) = \mathbf{E}\left\{\left(\sum_{d=1}^{U} x_d(t)\right)^2\right\} = \frac{E(N-2)}{2N}\left(2 - \frac{1}{2^{U-1}} + 4\Theta^2(0)\sum_{d_1=1}^{U}\sum_{\substack{d_2=1 \\ d_1 \neq d_2}}^{U}\frac{1}{\sqrt{2^{d_1+d_2}}}\right) \tag{13}$$

The received signal at the destination terminal is therefore

$$y(t) = Rx(t) \otimes h_{SD}(t) + v(t) \tag{14}$$

At the destination side, once the positive and negative sequences are received, the signal undergoes passes through parallel to serial conversion, removal of the cyclic prefix and DFT process. The received data without CP is used for signal combining. This combining process is done by subtracting the negative sequences from the positive sequences and this operation result in a 3 dB noise gain. The data encoded in all layers (depths) are demodulated iteratively. For the demodulation and symbol detection process, the data from first depth is recovered using the basic demodulator for U-OFDM. At this stage, the data is free from interference resulting from second depth to higher depths. The data from depth 1 can be optimally detected by applying *maximum likelihood (ML)* decision rule.

Similarly, the demodulation of data from second depth is unaffected by data from higher depths. However, the previous data (data from depth 1) interfere with data from second layer. Thus the estimated symbols from first depth are re-modulated and passed through the estimated channel. The resulting signal is then used to remove the ISI contribution from first depth prior to detecting of data symbols from depth 2 using U-OFDM demodulator and *ML* rule. The process continues until data from all depths are recovered. Figure 8 presents the iterative demodulation process for a maximum depth of 3.

### 2.2.2 Relay-Assisted Transmission

For the relay-assisted system, we consider the orthogonal amplify-and-forward relaying protocol described in [35]. This protocol operates in half-duplex mode and it consists of two time slots: the broadcasting phase and the relaying phase. During the first time slot, the source broadcast the signal to both relay and destination terminals. During the relaying phase, the source remains silent while the relay amplifies and forwards its received signal to the destination terminal. The received signals during the broadcasting phase at the destination and relay are written as

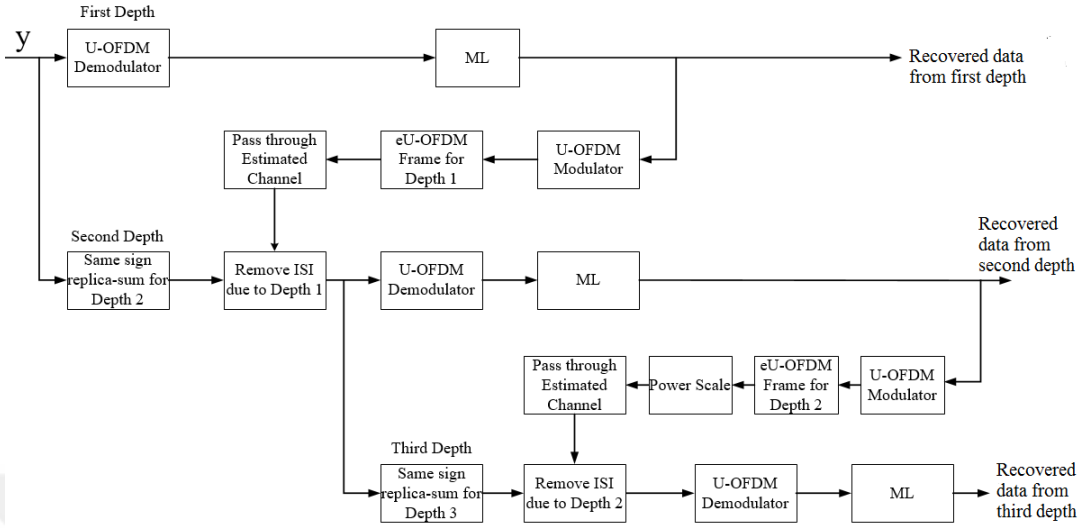


**Figure 8:** eU-OFDM iterative demodulator.

$$y_{D1}(t) = Rx(t) \otimes h_{SD}(t) + v_{D1}(t) \tag{15}$$

$$y_R(t) = Rx(t) \otimes h_{SR}(t) + v_R(t) \tag{16}$$

where $v_{D1}(t)$ and $v_R(t)$ are the corresponding AWGN with variance $\sigma_N^2$.

During the second time slot, the relay terminal amplifies the received signal by a factor of $G_A$ and forwards it to the destination. The received signal during this relaying phase is give as

$$y_{D2}(t) = RG_A y_{D1}(t) \otimes h_{SD}(t) + v_{D2}(t) \tag{17}$$

where $v_{D2}(t)$ is the AWGN with variance $\sigma_N^2$ and the amplification factor $G_A$ is given by

$$G_A = \sqrt{\frac{E_T(U)}{E_T(U)R^2 \sum\limits_n |h_{SR}(nTs)|^2 + \sigma_N^2}} \tag{18}$$

At the destination terminal, after $P/S$ conversion, removal of cyclic prefix and DFT process, the signal is decoded based on the following $ML$ rule defined in (19).

$$\hat{X}[k] = \arg\min_{x_i} \left[ \|Y_{D1}[k] - w_1[k]x_i\|^2 + \frac{1}{1 + |w_3[k]|^2} \|Y_{D2}[k] - w_2[k]w_3[k]x_i\|^2 \right] \tag{19}$$

where $w_1[k] = \sqrt{E}RH_{SD}[k],\ w_2 = \sqrt{E}RH_{SR}[k]$ and $w_3[k] = RG_AH_{RD}[k]$.

In the above expressions, $Y[k]$ and $H[k]$ denote respectively the DFT of the received signals and the channel impulse responses on on $k^{th}$ subcarrier where the subscripts are dropped for convenience. They can be written as

$$Y[k] = \frac{1}{\sqrt{N}} \sum_{n=0}^{N-1} y[n] e^{-j\frac{2\pi nk}{N}} \tag{20}$$

$$H[k] = \sum_{n=0}^{N-1} h[n] e^{-j\frac{2\pi nk}{N}} \tag{21}$$

## *2.3 Performance Analysis*

In U-OFDM transmission, when the average symbol energy is set to $E$, after Hermitian symmetry and IDFT processes, the energy becomes $E(N-2)/N$. Since the positive sub-frames and negative sub-frames (obtained after inverse in polarity prior to clipping) of the signal are transmitted separately and whenever the positive or negative sequences are set to zero, the transmitted signal energy is halved and becomes $E(N-2)/2N$. In eU-OFDM system, let the bipolar signal energy in the first depth be denoted by $E = E(N-2)/N$. The energies in the second depth, third depth, fourth depth and fifth depth are set to $E/2$, $E/4$, $E/8$ and $E/16$ by scaling the amplitude inversely proportional to $2^{d-1}$ where $d$ indicates the depth value. Hence, received symbol energy becomes $E$ in all depths at the output of the combining process in ideal channel conditions. After conversion of bipolar signal to positive signal, the energy in each depth scales by $1/2$ and the total signal energy gives the total energy $E_T(U)$ for a maximum depth of $U$.

For point-to-point transmission, the SNR per subcarrier for first depth is defined as

$$SNR_{Direct}[k] = \frac{ER^2|H_{SD}[k]|^2}{2\sigma_N^2} \tag{22}$$

For relay-assisted transmission, the $SNR$ per subcarrier for first depth is given by

$$SNR_{AF}[k] = \frac{ER^2|H_{SD}[k]|^2}{2\sigma_N^2} + \frac{ER^4G_A^2|H_{SR}[k]H_{RD}[k]|^2}{2\sigma_N^2\left(1+R^2G_A^2|H_{RD}[k]|^2\right)} \tag{23}$$

The overall average BER for (22) and (23) can be obtained by

$$BER = \frac{2}{N-2}\sum_{k=1}^{\frac{N}{2}-1} BER_{SC}[k] \tag{24}$$

where $BER_{SC}$ refers to BER per subcarrier and it is defined as (25)

$$\mathrm{BER_{SC}}[k] \approx \left\{ \begin{array}{ccc} Q\left(\sqrt{2\mathrm{SNR}}\right) & , & 2-\mathrm{PSK} \\ \frac{2\left(\sqrt{M}-1\right)}{\sqrt{M}\log_2\sqrt{M}}Q\left(\sqrt{\frac{3\mathrm{SNR}}{(M-1)}}\right) & , & \mathrm{square}-M-\mathrm{QAM} \\ \frac{2}{\log_2(U\mathrm{x}J)}\left[\frac{U-1}{U}Q\left(\sqrt{\frac{6\mathrm{SNR}}{U^2+J^2-2}}\right)+\frac{J-1}{J}Q\left(\sqrt{\frac{6\mathrm{SNR}}{U^2+J^2-2}}\right)\right] & , & \mathrm{rectangular}-M=U\mathrm{x}J-\mathrm{QAM} \end{array} \right\} \tag{25}$$

With reference to [26], the BER performance improves with increase in SNR values. As a result, the BER performances of all higher depths ($d > 1$) will start converging towards the BER performance of first depth. Consequently, we use ( 22) and (23) to estimate the BER of eU-OFDM based VLC system at high SNR values.

## *2.4 Numerical Results*

This section presents the numerical results of point-to-point and relay-assisted transmissions for the proposed eU-OFDM based VLC system. It also highlights their respective analysis in term of performance gains. The simulation parameters used in computing the numerical results are summarized in Table 1. For validation purpose, theoretical BER of the first depth for both direct and relay-assisted transmissions have been carried out. These results match perfectly with their Monte Carlo simulations. Throughout the simulations, we assume that both relay terminal and the optical receiver have perfect knowledge of the channel state information (CSI). The channel impulse responses presented in Figure 4 - Figure 6 are used in Monte Carlo simulation of the two systems.

The simulation and theoretical results for both relay-assisted and point-to-point systems are shown in Figure 9 and 10.

**Table 1:** Simulation Parameters for Single User VLC System

| | |
|---|---|
| Transmit and receive filters | SRRC |
| Excess bandwidth parameter | 1 |
| Sampling interval | 50 nsec |
| Power spectral density of noise | $10^{-22}$ W/Hz |
| Responsivity of photodetector | 0.54 A/W |
| OFDM frame duration | 3.2 $\mu$m |
| Cyclic prefix duration | 0.2 $\mu$m |
| Maximum depth value | 5 |

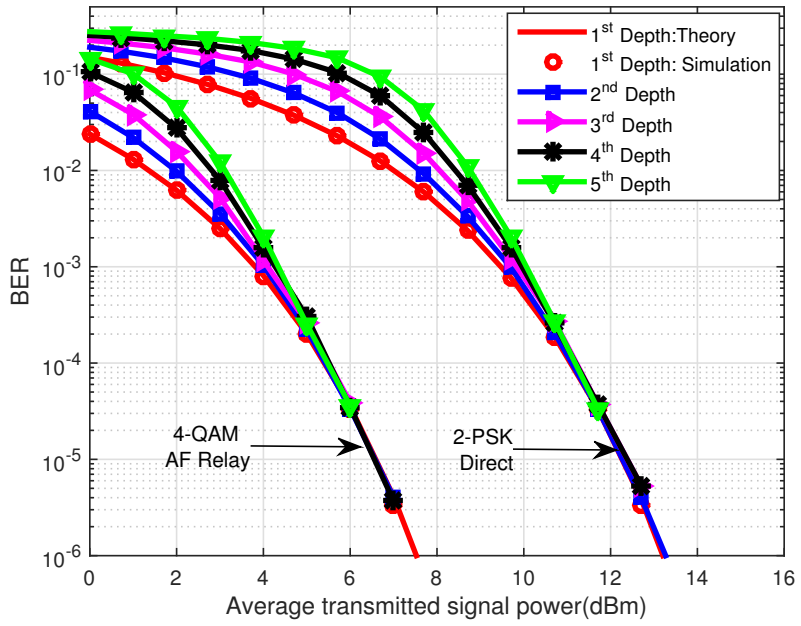


**Figure 9:** BER performance of eU-OFDM based VLC system with BPSK and 4-QAM

Figure 9 depicts the BER performance of point-to-point and relay-assisted systems. For the purpose of generating the same throughput for both systems, 2-PSK modulation scheme is used for direct transmission and 4-QAM is employed in relay-assisted transmission. This is to compensate for the half-duplex operation of the relaying protocol in which the transmission of data symbol is accomplished through two distinct time slots. However, in case of direct transmission, the data symbol is transmitted in a single time slot. Therefore, this modulation strategy will generate

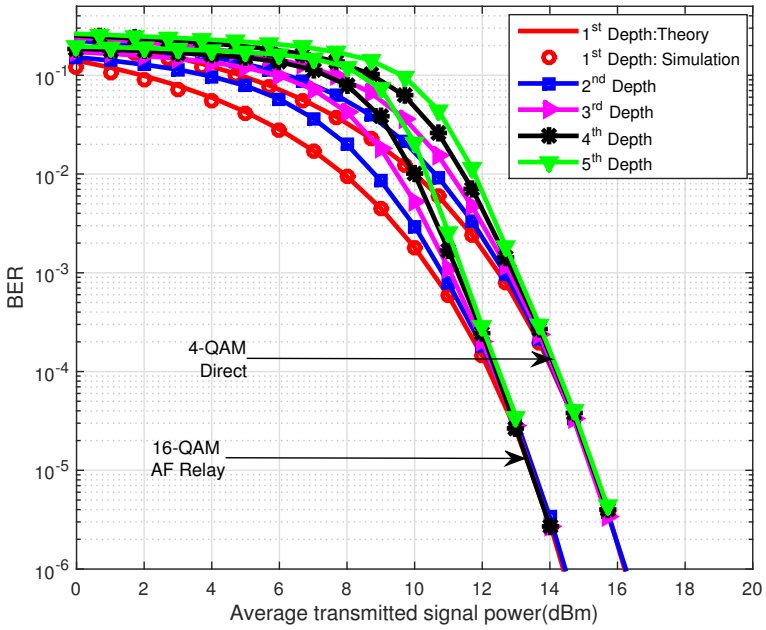


**Figure 10:** BER performance of eU-OFDM based VLC system with 4-QAM and 16-QAM

the same bit rate for both systems for a fair comparison. The expressions of BER from (24) and (25) are plotted in solid red color.

The BER performance of first depth is the same as the BER performance of U-OFDM [27]. Moreover, as expected from [26], the BER performances of all depths converge towards the performance of the first depth. The differences in BER at the lower values of SNR are due to the accumulated interference from previous depth as a result of their respective incorrect estimation at low SNR. The effects of interference are completely removed at high SNR which explains the convergence at this region. Monte Carlo simulations for all five depths are also plotted for direct and relay-assisted transmissions, the simulation results of the first depth matches with their respective theoretical counterparts.

In order to achieve a BER performance of $10^{-5}$, an average energy of 12.26 dBm

and 6.63 dBm are required for point-to-point and relay-assisted transmissions, respectively. Consequently, relay-assisted VLC system provides a gain improvement of 5.63 dBm.

Similarly, in Figure 10, we consider 4-QAM for point-to-point system and 16-QAM for relay-assisted scheme. As a result, at BER of $10^{-5}$, a performance gain of 1.79 dBm is observed. Compared to the previous scenario depicted in Figure 9, this performance is relatively low. This is due to the increase in constellation size.

# CHAPTER III

# eU-OFDM BASED MULTI-HOP VLC

In this chapter, a relay-assisted multi-hop VLC network is presented and analyzed. The network architecture is based on eU-OFDM and two configurations are adopted for the performance evaluation of the proposed serial multi-hop VLC link. With respect to this network topology, the signal-to-noise ratio of any user node within the multi-hop VLC network is derived and its BER expression is also presented. Through Monte Carlo simulation and theoretical performance analyses, we verify the validity of the relay-assisted multi-hop VLC system.

## *3.1 Channel Model*

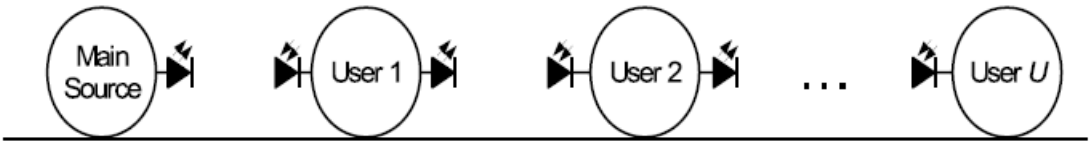


**Figure 11:** Multi-hop VLC network topology

The serial multi-hop VLC network topology used in this study is depicted in Fig. 11. It is assumed that the main source node and $U$ users are located sequentially and the transmission is based on LOS link. The LOS characteristic of the VLC channel is given by [10]

$$h = \left\{ \begin{array}{cc} \frac{a+1}{2\pi d^2}\cos^a(\phi)\cos(\psi) & 0 \leq \psi \leq \Psi_{\frac{1}{2}} \\ 0 & \psi \geq \Psi_{\frac{1}{2}} \end{array} \right\} \tag{26}$$

where $\phi$ denotes the irradiance angle with respect to the LED axis, $\psi$ is the angle of incidence with respect to PD axis, $d$ is the distance between LED and PD, $a =$

$-\ln(2)\Big/\ln\left(\cos\left(\Phi_{\frac{1}{2}}\right)\right)$ where the LED semi-angle $\Phi_{\frac{1}{2}}$ is set to 60°, the field-of-view (FOV) semi-angle of the photodetector $\Psi_{\frac{1}{2}}$ is assumed to be 60°.

## *3.2 System Model*

For the above network topology, we consider the eU-OFDM combined with QAM and PSK modulation schemes of constellation size $M$. The size of the modulated data symbols is again similar to that of U-OFDM $(N/2-1)$. Thus prior to IDFT of size $N$, the stream of modulated complex data symbols are subjected to Hermitian symmetry in order to obtain real value signals as described in **Section 2.2.1**. For convenience, we will use the eU-OFDM based system definition from **Section 2.2.1**.

### 3.2.1 Multi-Hop VLC Link: Configuration 1

We consider an eU-OFDM system with maximum depth of $U$. Let $x(t)$ denote the resulting time domain signal after summation of all depths. $E_T(U)$ denotes its energy and is given by (13).

Based on eU-OFDM frame structure, in order to serve $U$ users with the proposed system architecture and under this configuration, an eU-OFDM frame of maximum depth $U$ needs to be considered. The encoded data from the first depth are intended for first user terminal, data from second depth is to be transmitted to second user and so on, and the last user receives data from $U^{th}$ depth.

At the first terminal, the received signal can be written as

$$y_1(t) = Rh_1x(t) + n_1(t) \tag{27}$$

where $R$ is the responsivity of photodetector (A/W), $n_1(t)$ is additive white Gaussian noise (AWGN) with zero mean and $\sigma_N^2$ variance at first user node and $h_1$ is the VLC channel from main source to the first user node.

The detection of data intended for this node is straightforward. The decision process for each OFDM frame starts right after getting both the positive and negative

sequences. The combining process, which is done through the subtraction of the negative sequence from the positive parts, consequently leads to noise enhancement by a factor of two, however, the effects of higher depths are cancelled out. After serial-to-parallel conversion, cyclic prefix removed and DFT process, the signal can be decided optimally with *Maximum Likelihood*.

The SNR per sub-carrier at first user terminal is given by

$$SNR_1[n] = \frac{R^2 E h^2}{2\sigma_N^2} \tag{28}$$

Under the assumption of proper and successful detection of symbols, its interfering contribution in the received data $y_1(t)$ is removed after passing the estimated data through the estimated channel. The data to be amplified and forwarded is given by

$$\hat{y}_1(t) = y_1(t) - Rh_1\hat{x}_1(t) \tag{29}$$

The positive parts and negative parts carrying the same information of the second depth are summed and moved to first depth, the third depth data form the second depth in the new frame and so on. A magnitude scaling of $\sqrt{0.5}$ is applied for the conservation of the energy during this transformation in eU-OFDM frame structure and the signal is amplified with a factor of $G_1$ in order to set the power level to $E_T(U)$.

The subtraction from (29) eliminates the contribution of the data in the original first depth (data for user 1) in the initial total eU-OFDM symbol energy ($E_T(U)$). Therefore, the new total eU-OFDM signal energy for the new frame is

$$E_T(U-1) = \frac{E(N-2)}{2N}\left[2 - \frac{1}{2^{U-2}} + 4\Theta^2(0)\sum_{d_1=1}^{U-1}\sum_{\substack{d_2=1 \\ d_1\neq d_2}}^{U-1}\frac{1}{\sqrt{2^{d_1+d_2}}}\right] \tag{30}$$

Assuming that the data symbols for first user are correctly detected and their interfering contribution is completely removed, the amplification factor at user terminal 1 is defined as

$$G_1 = \sqrt{\frac{E_T(U)}{R^2 E_T(U-1)\,{h_1}^2 + \sigma_N^2}} \tag{31}$$

At the second user terminal, the received signal is given by

$$y_2(t) = RG_1 h_2 \hat{y}_1(t) + n_2(t) \tag{32}$$

where $n_2(t)$ is additive white Gaussian noise (AWGN) with zero mean and variance of $\sigma_N^2$ in the second node and $h_2$ is optical channel between first and second users.

The similar demodulation and detection processes used at first user terminal are applied for the detection and estimation of data for this second user.

At this second user terminal, SNR per sub-carrier is given by

$$SNR_2[n] = \frac{R^4 {G_1}^2 E {h_1}^2 {h_2}^2}{2\sigma_N^2 \left(R^2 {G_1}^2 {h_2}^2 + 1\right)} \tag{33}$$

The amplification factor at second user node is given by

$$G_2 = \sqrt{\frac{E_T(U)}{R^4 E_T(U-2) {h_1}^2 {h_2}^2 + \sigma_N^2 \left(R^2 G_1^2 {h_2}^2 + 1\right)}} \tag{34}$$

where $E(U-2)$ is obtained by using the same approach as in (30).

After subtraction of estimated symbols for user from $y_2(t)$, the resulting new data is then amplified by the factor of $G_2$ and forwarded to next user terminal. This data undergoes also the eU-OFDM frame reconstruction similar to that of the previous terminal.

This process continues until all the users terminals receives successfully their respective data. In respect to this, received signal at the $i^{th}$ terminal can be written as

$$y_i(t) = RG_{i-1} h_i \hat{y}_{i-1}(t) + n_i(t) \tag{35}$$

where $\hat{y}_{i-1}(t) = y_{i-1}(t) - Rh_{i-1}\hat{x}_{i-1}(t)$.

### 3.2.2 Multi-Hop VLC Link: Configuration 2

In this configuration, we consider the same data to be transmitted from the main source to all user nodes within the serial multi-hop network. The main source transmits the resulting eU-OFDM time domain signal to the first user node only.

This user terminal decodes the received signal but also amplifies it and forwards it to the next user. The second user applies the same decoding and relaying techniques used at the first user terminal. The process continues until the $U^{th}$ user node receives the original data sent from the main source. Thus, at the $U^{th}$ user terminal, the data undergoes $U-1$ amplification processes while travelling through $U$ LOS channels. Similar to *Configuration 1*, we consider an eU-OFDM signal of maximum depth $U$ and $x(t)$ (with average energy $E_T(U)$ as defined in ( 13)) its resulting time domain signal after summing signals from all depths.

Based on this configuration, the received time domain signal at the first user terminal is given by

$$y_1(t) = Rh_1 x(t) + n_1(t) \tag{36}$$

where $n_1(t)$ is the AWGN noise term with variance of ${\sigma_N}^2$.

The first User node decodes the signal after receiving both positive and negative sequences of the transmitted data. After P/S conversion, removal of CP, the negative sequences are subtracted from their respective positive sequences. Then user node 1 employs U-OFDM demodulation followed by *ML* detection rule to estimate the data. The expression of the SNR per subcarrier (for first depth) at this first user node is the same as (28). However, the amplification factor is defined as follow

$$G_1 = \sqrt{\frac{E_T(U)}{E_T(U) R^2 h_1^2 + \sigma_N^2}} \tag{37}$$

The time domain signal $y_1(t)$ is then amplified by a factor $G_1$ and forwarded to user terminal 2. The received signal at this user node is given by

$$y_2(t) = RG_1 h_2 y_1(t) + n_2(t) \tag{38}$$

where $n_2(t)$ has the same statistics as $n_1(t)$.

User node 2 decodes the signal using the iterative eU-OFDM demodulation approach, decoding and detection technique described in Chapter II. The expression of

the SNR per subcarrier (for first depth) of this user node is again the same as (33) but the amplification factors of user node 2 based on *Configuration 2* is given as

$$G_2 = \sqrt{\frac{E_T(U)}{E_T(U) R^4 G_1^2 h_1^2 h_2^2 + \sigma_N^2 (R^2 G_1^2 h_2^2 + 1)}} \tag{39}$$

The second user terminal amplifies $y_2(t)$ and forwards it to the third user. This process continues till all user terminals receive the signal transmitted from the main source. Consequently, at $i^{th}$ user terminal, the received time domain signal is given by

$$y_i(t) = RG_{i-1} h_i y_{i-1}(t) + n_i(t) \tag{40}$$

## 3.3 Performance Analysis

Under the assumption that the symbols on each depth are perfectly decided, the generalized SNR formula for the $i^{th}$ user node can be derived.

At $i^{th}$ user node, the amplification is defined as

$$G_i = \sqrt{\frac{E_T(U)}{R^{2i} E_i(U) \prod_{k=1}^{i} h_k^2 + \sigma_N^2 (1 + \alpha_i + \alpha_i\alpha_{i-1} + \alpha_i\alpha_{i-1}\alpha_{i-2} + ...)}} \tag{41}$$

where $\beta_i$ is equal to $\alpha_i + \alpha_i\beta_{i-1}$ in which $\alpha_i = R^2 G_{i-1}^2 h_i^2$ for $i \in \{2, ..., U\}$ and 0 for $i \in \{0, 1\}$ with initial definitions of $\beta_0 = 0$ and $G_0 = 1$, and $E_i(U)$ is defined as follow

$$E_i(U) = \begin{cases} E_T(U - i) & \text{for } \textit{configuration 1} \\ E_T(U) & \text{for } \textit{configuration 2} \end{cases} \tag{42}$$

Therefore, by using the definitions of $\beta_i$ and $\alpha_i$, the expression of $G_i$ can be simplified as follow

$$G_i = \sqrt{\frac{E_T(U)}{R^{2i} E_i(U) \prod_{k=1}^{i} h_k^2 + \sigma_N^2 (1 + \beta_i)}} \tag{43}$$

Similarly, the generalized SNR can be written as

$$\mathrm{SNR}_i = \frac{R^{2i} E \prod_{k=1}^{i} {h_k}^2 G_{k-1}^2}{2\sigma_N^2 \left(1 + \alpha_i + \alpha_i\alpha_{i-1} + \alpha_i\alpha_{i-1}\alpha_{i-2} + ...\right)} \tag{44}$$

Through variable change with respect to $\beta_i$ and $\alpha_i$, the SNR becomes

$$\mathrm{SNR}_i = \frac{R^{2i} E \prod_{k=1}^{i} h_k^2 G_{k-1}^2}{2\sigma_N^2 \left(1 + \beta_i\right)} \tag{45}$$

Relatively, BER [36] can be written as (25).

As the SNR increases, the BERs on previous nodes decrease and the performances of all depths converge to analytical results [26]. Therefore, (24) and (25) can be used to estimate BER of eU-OFDM system at high SNR values.

## *3.4 Numerical Results*

In this Section, we present numerical results to confirm the analytical SNR and BER expressions. Simulation parameters are defined in Table 2. In all the simulations, we assume that perfect channel state information is available at all nodes. We consider a scenario including one main source and three users. For *Configuration 1*, we consider an eU-OFDM with maximum depth of 3. For the second configuration, we consider a maximum depth of 1 for convenience. In addition, equal distance between VLC nodes is assumed throughout these performance analyses.

**Table 2:** Simulation Parameters for Multi-Hop VLC system

| | |
|---|---|
| Sampling interval | 50 nsec |
| Noise power ($\sigma_N^2$) | -35 dBm |
| Responsivity of photodetector | 0.54 A/W |
| OFDM frame duration | 3.2 $\mu$m |
| Cyclic prefix duration | 0.2 $\mu$m |
| Distance between VLC nodes | 2 m |
| Maximum depth value | 3, 1 |

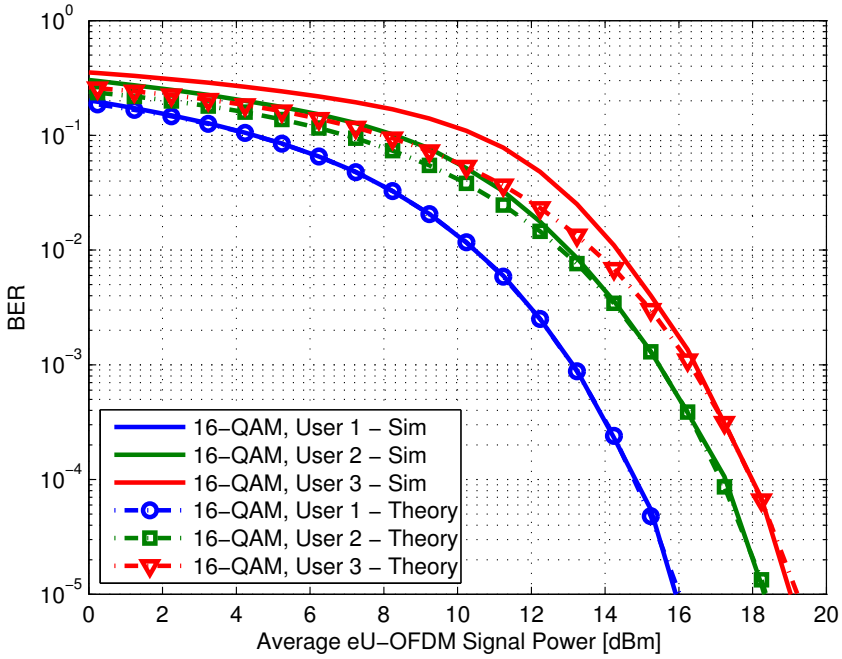


**Figure 12:** BER with respect to average signal energy when 16-QAM is used for all users (*Configuration 1*)

In Figure 12, we present the BER results obtained through both theoretical and Monte Carlo simulations, *configuration 1* is considered in this case. 16-QAM is selected as modulation scheme for each depth. Therefore, the throughput gradually decrease for each node. It can be seen that since interference from higher depths are perfectly cancelled out, the BER results are matched with analytical expression for first user.

Additionally, in order to get $10^{-3}$ BER, 13.12 dBm of eU-OFDM average signal power is required. This level increases to 15.45 dBm for second user and 16.32 dBm for third user. The increment of the required power level is due to both noise amplification in each node and channel attenuation. However, the differences between these levels gradually decrease and this is because when each node extract its information, the remaining data are transmitted with higher energy with respect to previous transmission.

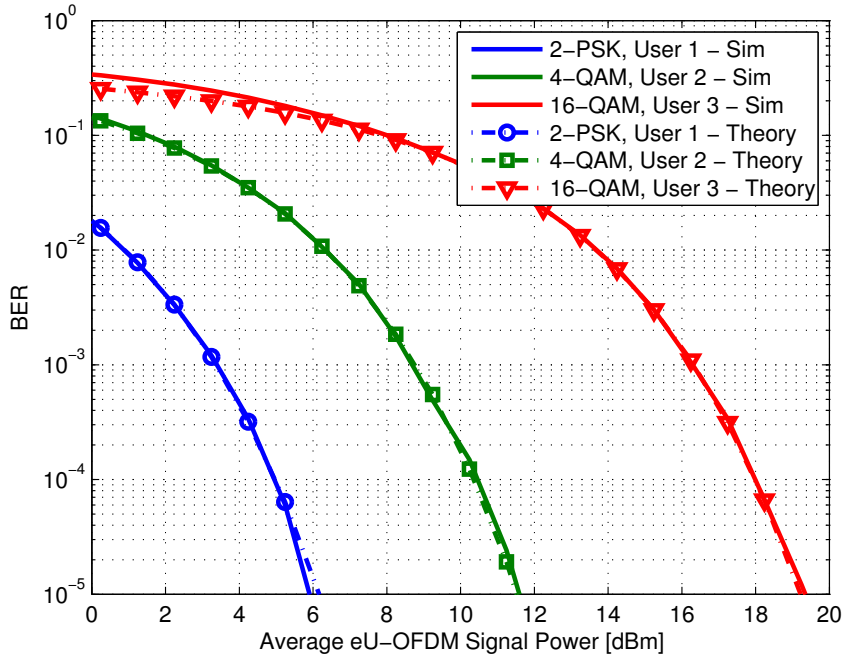


**Figure 13:** BER with respect to average signal energy for equal throughput among all users (*Configuration 1*)

Also, it should be noted that simulation and theoretical results for second and third users converge towards to each other in high SNR region. The difference observed at low SNR region is due to incorrect decision on symbols in previous users which leads to imperfect interference cancellation in the subsequent nodes.

In Figure 13, we present BER results for a scenario in which all users have equal throughput. In this scenario, *Configuration 1* is again being considered. For equal throughput among all three user nodes, we set the modulation schemes for the first, second and third users to 2-PSK, 4-QAM and 16-QAM, respectively. At a targetted BER of $10^{-3}$, the required average eU-OFDM signal power for the first user is 3.4 dBm. This value increases to 8.7 dBm and 16.3 dBm for second and third users due to deployment of higher modulation orders.

In the following figures, we present the BER performance for three user nodes. The bit error rate performances of the proposed relay-assisted multi-hop VLC network

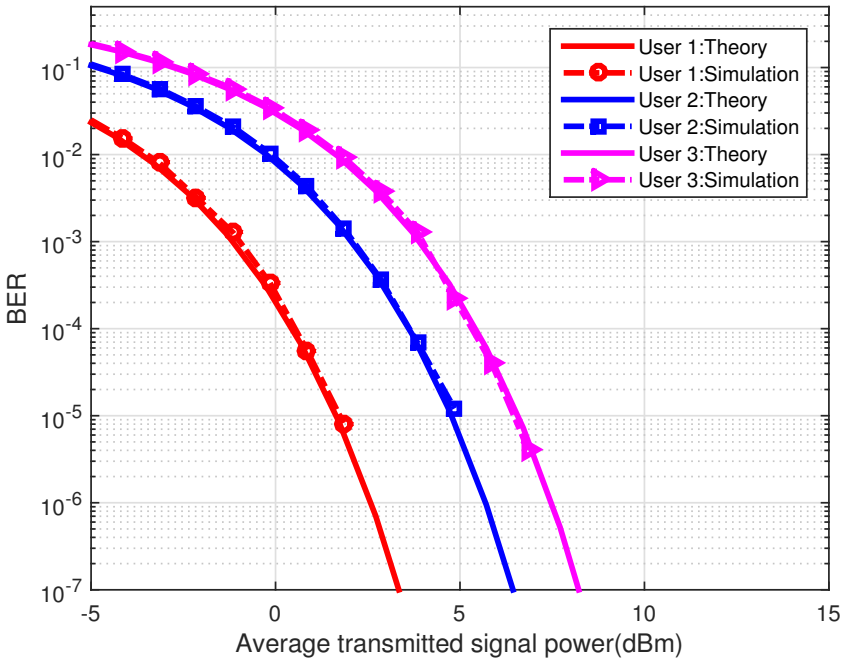


**Figure 14:** BER vs average signal energy when 2-PSK is used (*Configuration 2*)

based on *configuration 2* are portrayed in Figure 14 and Figure 15. For clarity and convenience, we have adopted eU-OFDM of maximum depth equal to unity. 2-PSK and 16-QAM modulation schemes are used in this performance analysis.

Figure 14 depicts the BER performance of three user nodes when 2-PSK modulation is used. For a BER of $10^{-4}$, an average signal power of 0.45 dBm is required for user terminal 1. This power requirement increases to 3.6 dBm and 5.4 dBm for second and third users, respectively. For each subsequent user node, additional power is required due to path loss of the visible light channel.

Similarly, in Figure 15, we present the BER performance of three user terminals by adopting a 16-QAM modulation scheme. As a result, the first, second and third user nodes required respectively average signal powers of 10.3 dBm, 13.3 dBm and 15 dBm in order to achieve a bit error rate performance of $10^{-4}$. Comparatively and based on Figure14 and Figure 15, the higher the complex modulation size, the more

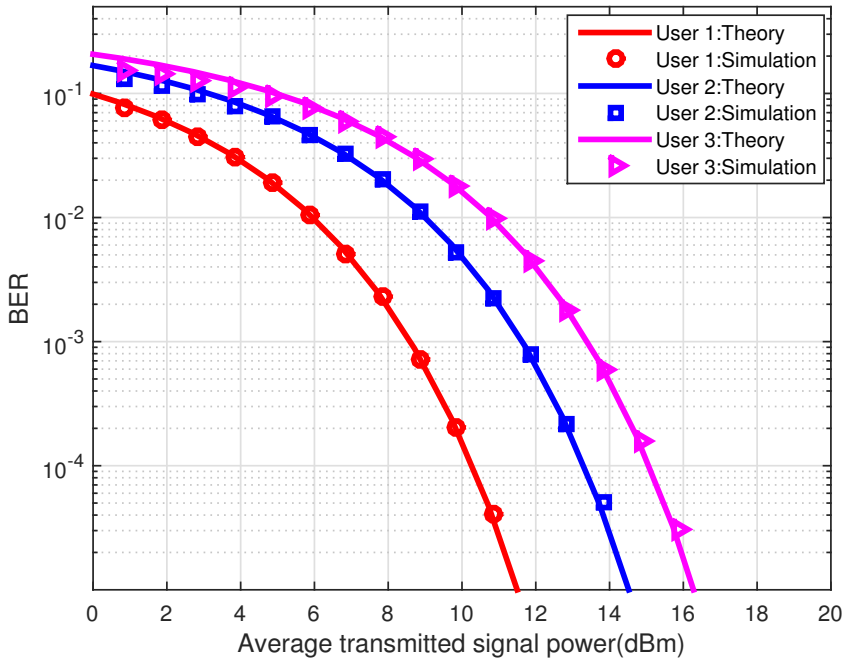


**Figure 15:** BER vs average signal energy when 16-QAM is used (*Configuration 2*)

average signal power is required.

In order to investigate the effects of path loss resulting from the visible light channel [5], we consider a scenario in which there are no relays between the main source and the third user terminals (or direct transmission), the distance from main source to this third user is set to 6 m. For the case employing *Configuration 2* of the relay-assisted multi-hop VLC, the equidistance between nodes is still kept at 2 m so that overall distance from the main source to the third user node gives 6 m. As shown in Figure 16, an average signal power of 5.4 dBm is required to achieve a BER of $10^{-4}$ at user terminal three when *Configuration 2* is used. On the other hand, for direct transmission, the third user will required an average signal power of 19.65 dBm in order to achieve the same BER performance. Consequently, the use of relay-assisted multi-hop VLC based on (*Configuration 2*) helps to cut down the transmit power by 14.25 dBm over a distance of 6 m.

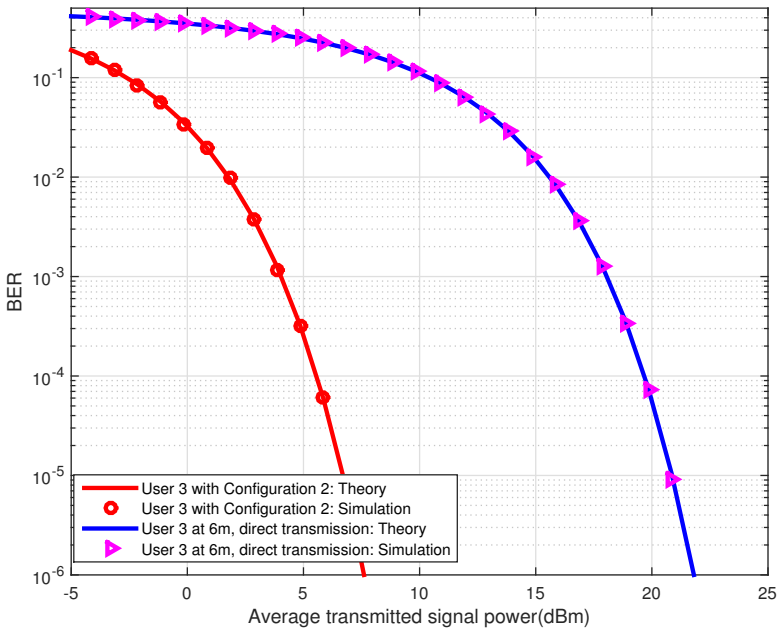


**Figure 16:** Effects of path loss on BER performance with 2-PSK

# CHAPTER IV

# CONCLUSION

Visible light communication is an evolving and emerging technology which will greatly alleviate the spectral burden on the current RF-based wireless systems. In this thesis, we have evaluated the performance of relay-assisted VLC systems based on enhanced unipolar OFDM by considering different network topologies for an indoor environment.

Based on the reference channel model adopted by IEEE 802.15.7r Task Group "Short Range Optical Wireless Communication", we have demonstrated that eU-OFDM based VLC system employing AF relaying protocol presents a superior performance compared to direct transmission. In addition, a relay-assisted multi-hop for eU-OFDM based VLC systems has been proposed and analyzed. We have derived the SNR and BER of user nodes based on two configurations of the serial multi-hop VLC network. For the first configuration, we have demonstrated that subsequent user nodes present a fairly poor BER performance with respect to their preceding user terminals when a 16-QAM modulation scheme is assumed for all users. Consequently, the throughput is reduced by half for each subsequent user terminal. In order to maintain the same throughput among all users, 2-PSK, 4-QAM and 16-QAM can be used respectively for the first, second and third users. However, this equal throughput among users leads the increment of the difference between required signal energy level for each user to achieve the same BER target. For the second configuration, we have also demonstrated that serial multi-hop VLC system using orthogonal amplify-and-forward relaying protocol can help to significantly reduce the required transmit power at the optical source.

# Bibliography


[1] S. M. Uysal, T. Baykas, F. Miramirkhani, N. Serafimovski, and V. Jungnickel, "Ieee p802. 15,"

[2] M. Uysal and H. Nouri, "Optical wireless communicationsan emerging technology," in *2014 16th International Conference on Transparent Optical Networks (ICTON)*, pp. 1–7, IEEE, 2014.

[3] M. A. Khalighi and M. Uysal, "Survey on free space optical communication: A communication theory perspective," *IEEE Communications Surveys Tutorials*, vol. 16, pp. 2231–2258, Fourthquarter 2014.

[4] G. J. Holzmann and B. Pehrson, *The early history of data networks*. IEEE Computer Society Press, 1995.

[5] F. R. Gfeller and U. Bapst, "Wireless in-house data communication via diffuse infrared radiation," *Proceedings of the IEEE*, vol. 67, pp. 1474–1486, Nov 1979.

[6] Z. Ghassemlooy, W. Popoola, and S. Rajbhandari, *Optical wireless communications: system and channel modelling with Matlab®*. CRC Press, 2012.

[7] S. Hranilovic, *Wireless optical communication systems*. Springer Science & Business Media, 2006.

[8] F. E. Goodwin, "A review of operational laser communication systems," *Proceedings of the IEEE*, vol. 58, pp. 1746–1752, Oct 1970.

[9] D. L. Begley, ""free-space laser communications: a historical perspective"," in *Lasers and Electro-Optics Society, 2002. LEOS 2002. The 15th Annual Meeting of the IEEE*, vol. 2, pp. 391–392 vol.2, Nov 2002.

[10] J. R. Barry, *Wireless infrared communications*, vol. 280. Springer Science & Business Media, 2012.

[11] S. Arnon, J. Barry, and G. Karagiannidis, *Advanced optical wireless communication systems*. Cambridge university press, 2012.

[12] S. S. Muhammad, T. Plank, E. Leitgeb, A. Friedl, K. Zettl, T. Javornik, and N. Schmitt, "Challenges in establishing free space optical communications between flying vehicles," in *Communication Systems, Networks and Digital Signal Processing, 2008. CNSDSP 2008. 6th International Symposium on*, pp. 82–86, July 2008.

[13] X. Zhu and J. M. Kahn, "Free-space optical communication through atmospheric turbulence channels," *IEEE Transactions on Communications*, vol. 50, pp. 1293–1300, Aug 2002.

[14] Z. Xu and B. M. Sadler, "Ultraviolet communications: Potential and state-of-the-art," *IEEE Communications Magazine*, vol. 46, pp. 67–73, May 2008.

[15] B. Weir, "Driving the 21st century's lights," *IEEE Spectrum*, vol. 49, pp. 42–47, March 2012.

[16] S. Wu, H. Wang, and C. H. Youn, "Visible light communications for 5g wireless networking systems: from fixed to mobile communications," *IEEE Network*, vol. 28, pp. 41–45, Nov 2014.

[17] M. B. Rahaim, A. M. Vegni, and T. D. C. Little, "A hybrid radio frequency and broadcast visible light communication system," in *2011 IEEE GLOBECOM Workshops (GC Wkshps)*, pp. 792–796, Dec 2011.

[18] T. D. C. Little, P. Dib, K. Shah, N. Barraford, and B. Gallagher, "Using led lighting for ubiquitous indoor wireless networking," in *2008 IEEE International Conference on Wireless and Mobile Computing, Networking and Communications*, pp. 373–378, Oct 2008.

[19] P. H. Pathak, X. Feng, P. Hu, and P. Mohapatra, "Visible light communication, networking, and sensing: A survey, potential and challenges," *IEEE Communications Surveys Tutorials*, vol. 17, pp. 2047–2077, Fourthquarter 2015.

[20] S. Singh, G. Kakamanshadi, and S. Gupta, "Visible light communication-an emerging wireless communication technology," in *2015 2nd International Conference on Recent Advances in Engineering Computational Sciences (RAECS)*, pp. 1–3, Dec 2015.

[21] V. Chandrasekhar, J. G. Andrews, and A. Gatherer, "Femtocell networks: a survey," *IEEE Communications Magazine*, vol. 46, pp. 59–67, September 2008.

[22] S. Dimitrov and H. Haas, *Principles of LED Light Communications: Towards Networked Li-Fi*. Cambridge University Press, 2015.

[23] B. E. Saleh, M. C. Teich, and B. E. Saleh, *Fundamentals of photonics*, vol. 22. Wiley New York, 1991.

[24] T. Komine and M. Nakagawa, "Fundamental analysis for visible-light communication system using led lights," *IEEE Transactions on Consumer Electronics*, vol. 50, pp. 100–107, Feb 2004.

[25] J. Armstrong and A. J. Lowery, "Power efficient optical ofdm," *Electronics Letters*, vol. 42, pp. 370–372, March 2006.

[26] D. Tsonev, S. Videv, and H. Haas, "Unlocking spectral efficiency in intensity modulation and direct detection systems," *IEEE Journal on Selected Areas in Communications*, vol. 33, pp. 1758–1770, Sept 2015.

[27] D. Tsonev, S. Sinanovic, and H. Haas, "Novel unipolar orthogonal frequency division multiplexing (u-ofdm) for optical wireless," in *Vehicular Technology Conference (VTC Spring), 2012 IEEE 75th*, pp. 1–5, May 2012.

[28] N. Fernando, Y. Hong, and E. Viterbo, "Flip-ofdm for unipolar communication systems," *IEEE Transactions on Communications*, vol. 60, pp. 3726–3733, December 2012.

[29] J. Armstrong, "Ofdm for optical communications," *Journal of Lightwave Technology*, vol. 27, pp. 189–204, Feb 2009.

[30] E. Lam, S. K. Wilson, H. Elgala, and T. D. Little, "Spectrally and energy efficient ofdm (see-ofdm) for intensity modulated optical wireless systems," *arXiv preprint arXiv:1510.08172*, 2015.

[31] J. N. Laneman, D. N. C. Tse, and G. W. Wornell, "Cooperative diversity in wireless networks: Efficient protocols and outage behavior," *IEEE Transactions on Information Theory*, vol. 50, pp. 3062–3080, Dec 2004.

[32] O. Narmanlioglu, R. C. Kizilirmak, and M. Uysal, "Relay-assisted ofdm-based visible light communications over multipath channels," in *2015 17th International Conference on Transparent Optical Networks (ICTON)*, pp. 1–4, July 2015.

[33] M. Uysal, "Performance analysis of dco-ofdm systems in the presence of realistic indoor visible light channels," 2015.

[34] R. C. Kizilirmak, O. Narmanlioglu, and M. Uysal, "Relay-assisted ofdm-based visible light communications," *IEEE Transactions on Communications*, vol. 63, pp. 3765–3778, Oct 2015.

[35] M. Uysal, *Cooperative Communications for Improved Wireless Network Transmission: Framework for Virtual Antenna Array Applications*. IGI Global, 2009.

[36] K. Cho and D. Yoon, "On the general ber expression of one- and two-dimensional amplitude modulations," *IEEE Transactions on Communications*, vol. 50, pp. 1074–1080, Jul 2002.

# VITA

Gerard Djengomemgoto completed his bachelor of science (BSc) in Electrical & Electronics Engineering at Universiti Teknologi PETRONAS, in Malaysia (2014). In the same year, he joined the Communication Theory & Technologies (CT&T) research group at Özyeğin University and started his Master's degree program under the supervision of Professor Murat Uysal. His research interest is in the areas of visible light and cooperative communications.